Effects of Various Surfactants on Alkali Lignin Electrospinning Ability and Spun Fibers

Charlton, Adam

Industrial & Engineering Chemistry Research

DOI:
10.1021/acs.iecr.7b02494

Published: 30/08/2017

Peer reviewed version

Effects of various surfactants on alkali lignin electrospinning ability and spun fibers

Wei Fang†, Sen Yang†, Tong-Qi Yuan†, *, Adam Charlton‡ and Run-Cang Sun†, *

† Beijing Key Laboratory of Lignocellulosic Chemistry, Beijing Forestry University, Beijing, 100083, P. R. China.

‡ The BioComposites Centre, Bangor University, Deiniol Road, Bangor, Gwynedd, LL57 2UW, UK

*Corresponding authors:

E-mail: ytq581234@bjfu.edu.cn, rcsun3@bjfu.edu.cn.

Fax: +86-10-62336903; Tel: +86-10-62336903.

ABSTRACT

Anionic, cationic, and non-ionic surfactants with varying concentrations (0.2 - 1.2 %)were introduced to neutralize beads on lignin nanofibers by decreasing the surface tension of spinning dopes. The surfactants used in this work were sodium dodecyl sulfate (SDS), N,N,N-trimethyl-1-dodecanaminium bromide (DTAB), and Triton™ X-100 (TX-100). The effects of viscosity, rheological properties, surface tension, and conductivity of the solutions on the morphology and physicochemical performances of fibers were investigated. As expected, the presence of certain amounts of surfactants eliminated the beads and resulted in the formation of smooth and bead-free fibers with small diameters. Furthermore, the gravimetric capacitance of carbon mat with 1 % SDS was slightly improved from 66.3 to 80.7 F g^{-1}. The results suggested that the surfactants benefit the electrospinning of lignin and allow for the control over nanofiber morphology without compromising their performance as supercapacitor electrodes.

KEYWORDS: *lignin, electrospinning, surfactant, carbon nanofiber, supercapacitor*

INTRODUCTION

As a variant of electrostatic spraying, electrospinning is a technique for forming continuous nanofibers with a high voltage supplier, a syringe, and a collector plate or drum.[1-4] The spinneret is connected to a syringe where the polymer solution (or melt) is hosted until being fed into the spinneret. After exposure to a high-voltage electric field, polymer solutions or melts are expelled from the syringe and solid fibers are deposited onto the collector. The high drawing rate or elongation (up to 1,000,000 s^{-1})[5] and solvent evaporation cause the fiber diameters to dramatically decrease from hundreds of micrometers to as small as tens of nanometers very quickly (within 50 ms). Since the revival of electrospinning in the 1990s,[6, 7] the technique has been extensively studied and applied in various fields including electric, catalysis, tissue engineering, and others.[8-11]

Lignin is composed of three monomer building blocks: *p*-hydroxyphenyl (H), guaiacyl (G), and syringyl (S).[12, 13] As the second most abundant biopolymer and the most abundant aromatic-containing polymer in nature, lignin has gained extensive interest for preparing certain valuable materials. The electrospinning of lignin has grown popular over the years since being first reported by Lallave et al.[14] as a convenient technique for producing nanofibers. Lignin-based nanofibers and carbon nanofibers have furthered advancements in response, battery, and supercapacitor applications.[15-17] For most cases, electrospinning of lignin requires the incorporation of other polymers.[14, 18, 19] For instance, PVA,[20-23] PEO,[24, 25] and PAN[26, 27] have been used to facilitate polymer entanglement and improve the electrospinning abilities of lignins.

The formation of lignin-based beaded fibers has been widely reported in the literature;[24, 26, 28] and many previous researchers have explored the formation of beaded fibers for other precursors. Fong et al.[29] suggested that the viscoelasticity and surface tension of the solution are the key factors influencing the formation of beaded fibers. Lin et al.[30] found that insufficient stretching of the polymer jet due to the weak charging forces can lead to the formation of the beaded fibers. For lignin electrospinning, beaded fibers are mainly attributed to the viscoelasticity of the solution.[25]

Surfactants are amphiphilic molecules containing hydrophilic and hydrophobic parts. Surfactants have numerous useful applications due to their ability to lower surface free energy and thus surface tension.[31] When used in the electrospinning, surfactants can 1) lower the surface tension of the solution; 2) enhance the conductivity of the solution in case of ionic surfactants; 3) modulate the molecular structure and interactions of polymers;[32] and 4) alter the rheology and viscoelasticity of the solution. All of these effects can prompt the formation of bead-free and thin fibers while assisting the electrospinning process.

There are four main types of surfactants used in the electrospinning technique: Anionic, cationic, non-ionic, and amphoteric ones. Lin et al.[30] found that the addition of cationic surfactant eliminates the beads on polystyrene fibers, but that the addition of non-ionic surfactant only reduces the number of beads. Bhattarai et al.[33] introduced non-ionic surfactant to improve both the spinnability of chitosan solution and the resulting fiber structure. The

effects of different types and contents of surfactants on the electrospinning of various polymer solutions have also been explored by several researchers.[32, 34-39]

This paper presented a simple and effective method to modulate the morphology and diameter of alkali lignin-based nanofibers by utilizing surfactants to tune the rheology and other properties of the spinning solutions. Various types (ionic, cationic, and non-ionic) and contents of surfactants were added into lignin-PVA solutions and the morphology and size of the as-spun fibers were assessed. It was found that the electrochemical properties of carbonized nanofibers as electrodes for supercapacitors were uncompromised by the addition of surfactants.

EXPERIMENTAL SECTION

Materials. Alkali lignin powder was purchased from Sigma-Aldrich (catalog number 471003) with average molecular weight of 10,000 and 4 % sulfur content. Poly (vinyl alcohol) (PVA) powder was also purchased from Sigma-Aldrich with molecular weight ranging from 85,000 to 124,000 and hydrolysis degree of 87-89%. Anionic surfactant sodium dodecyl sulfate (SDS) was purchased from Aladdin (catalog number 108347). Cationic surfactant N,N,N-trimethyl-1-dodecanaminium bromide (DTAB) was also purchased from Aladdin (catalog number 105301). Non-ionic surfactant Triton™ X-100 (TX-100) was obtained from Sigma-Aldrich (catalog number 900502). All chemicals were used as-received without further purification.

Electrospinning. First, 0.7 g alkali lignin was dissolved in 9 g deionized water by stirring at room temperature, and 0.3 g PVA powder was then added to the aqueous solution under stirring. The resulting mixture was heated to 75 °C and stirred continuously until the PVA was totally dissolved. Next, the surfactants were added to the cooled solution and stirred for 1 h to prepare spinning dopes with surfactant mass percentages of 0.2, 0.4, 0.6, 0.8, 1.0, and 1.2. The dopes were loaded into a plastic syringe attached to a 22G needle (inner diameter of 0.41 mm) and spun with an electrospinning machine (JFD 04, Nayi Instruments, Changsha, China). The electrospinning conditions included an applied voltage and distance between the needle and collector of 22 kV and 15 cm, respectively. The feeding rate was 1 mL h^{-1} and the collector drum rotating speed was 300 rpm. The as-spun nanofiber membranes were finally vacuum dried at 60 °C overnight.

Stabilization and Carbonization. Some of the spun membranes (control, 1% SDS, 1% DTAB, 1% TX-100) were stabilized and carbonized to test the effects of surfactant addition on the electrochemical properties of the carbonized mats. The membranes were attached to a copper mesh with adhesive tape (heat-resistant up to 280 °C) and placed in a tube furnace (SK-G08123K, Zhonghuan Furnace, Tianjin, China). The heating procedure was taken from the literature[40] as follows: 1) The temperature was increased from 25 to 105 °C at 5 °C min^{-1} then 2) held at 105 °C for 1 h, 3) increased from 105 to 180 °C at 1 °C min^{-1}, 4) held for 16 h, 5) increased from 180 to 220 °C at 0.5 °C min^{-1}, 6) held for 6 h, then 7) naturally cooled down to room temperature. A constant air flow was maintained during the whole process.

The stabilized membranes were placed in a quartz boat and carbonized under nitrogen flow in the same tube furnace. The heating process was as follows: 1) Temperature was increased from 25 to 900 °C at 5 °C min^{-1}, then 2) held for 1 h and 3) naturally cooled down to room temperature. The carbonized nanofiber membranes were washed with deionized water three times to remove any impurities and vacuum dried at 60 °C overnight. The carbonized mats were labeled as CNF-C, CNF-SDS, CNF-DTAB, and CNF-TX for fibers spun from solutions without surfactant, 1.0 % SDS, 1.0 % DTAB, and 1.0 % TX-100, respectively.

Characterization. The apparent viscosity of the solution was measured with a viscometer (DV II+ Pro, Brookfield, USA). The rheological properties were recorded on a rheometer (MCR 301, Anton Paar, Austria), and shear stress σ (Pa) was recorded as a function of shear rate (s^{-1}) ranging from 10^{-3} to 10^{3} s^{-1}. Solutions were equilibrated to 25 °C prior to all measurements. Measurements were fitted to the power law model:[32, 41]

$$\sigma = K\,\gamma^{n} \quad (1)$$

where *K* is the consistency coefficient and *n* is the flow behavior index. If the flow behavior index *n* equals 1, the solution behaves as a Newtonian liquid. If it is smaller than 1, the solution is a shear thinning liquid; if it is larger than 1, the solution is shear thickening.

The surface tension and conductivity of each solution was measured with a fully automatic surface tension meter (QBZY, Fangrui Instruments, Shanghai, China) and a portable analytic instrument with a portable analyzer (HQD 40, Hack Instruments, USA), respectively.

The morphology of the resulting membranes was examined with a scanning electron microscope (SEM, HitachiS-5500). The average diameter and diameter distribution were measured with image analysis software (ImageJ, NIH, USA) from >50 randomly selected fibers for each sample.

The FT-IR spectra of nanofiber membranes were collected on a Thermo Scientific Nicolet iN 10 FT-IR Microscopy (Thermo Nicolet Corp., Madison, WI) equipped with a liquid nitrogen cooled MCT detector. Thirty-two scans were taken for each sample with a resolution of 4 cm^{-1} in the reflection mode. Each sample was spread on a plate before spectra collection.

Differential scanning calorimetry (DSC) characterization was carried out with a differential scanning calorimeter (DSC 214 Polyma, NETZSCH-Gerätebau GmbH, Selb, Germany). Samples of approximately 5 mg were loaded into DSC pans and then equilibrated at 25 °C for 5 min before heating from 25 to 300 °C at a rate of 5 °C min^{-1}. The temperatures of samples and reference pans were measured as a function of oven temperature to determine the heat flow. The results reported here are an average of three measurements.

A symmetrical two-electrode cell was assembled as prototype supercapacitor using carbonized mats as electrodes (size ~ 1.0 cm^2) without any polymeric binder or conductive additive. Two pieces of platinum sheet were used as current collectors. Electrochemical characterizations including cyclic voltammetry (CV) and galvanostatic charge/discharge of the CNF membranes were conducted with a two-electrode cell in 6M KOH aqueous solution with

an electrochemical workstation. CV studies were performed at scanning rates from 5 to 2000 mV s^{-1} within the voltage window from 0 to 1 V.

RESULTS AND DISCUSSION

Apparent Viscosity of the Solution. The apparent viscosities of solutions with surfactants of varying types and contents were measured under a constant shear rate of 50 s^{-1} (Fig. 1). The lignin-PVA solution showed an apparent viscosity of 241.1 mPa s. The addition of small amounts of each surfactant reduced the viscosity of the solution. After introducing 0.2 % SDS, DTAB, or TX-100, the viscosity of the solution decreased to 216, 174, and 158.8 mPa s, respectively. Viscosity has a marked impact on the size of nanofibers,[25, 42] therefore the diameter of fibers can be adjusted by simply adding surfactants accordingly. However, the viscosity increased as SDS content increased while the parameter continued to decrease as further adding DTAB and TX-100. The viscosity of the solutions with 0.8 - 1.2 % SDS even surpassed the value of the solution without surfactant.

Different variation trends in viscosity may be attributable to the varying strength patterns of the surfactant-polymer interaction depending on the chemical properties of the polymer and surfactant.[43-45] Ionic surfactants could bind cooperatively to non-ionic polymers once the content surpasses its critical micelle concentration (cmc)[34] which, in this case, was PVA (Fig. 2). This cooperative binding, driven by electrical or hydrophobic interactions, led to the formation of surfactant-polymer complexes. For PVA-only solutions, such complexes formed as the incorporated ionic surfactants strongly interacted with the alkyl groups thus increasing

the viscosity.[34] In the presence of alkali lignin, the anionic group containing polymers (cationic surfactant, DTAB) interacted with lignin through electrostatic force upon reaching its cmc (approximately 0.5 %). The viscosity continued to decrease as the DTAB content increased. Because there was no such electrostatic force between SDS and lignin, the hydrophobic interactions among the surfactant, lignin, and PVA formed the compounds and hence increased the viscosity. For non-ionic surfactant (TX-100), there was no cooperative binding due to the non-ionizing properties, and the viscosity of its solution decreased as the content increased.

Rheology of the Solution. Next, solutions with all surfactants of several concentrations (0, 0.2, 0.6, 1.0 %) were explored for their rheological properties. Flow curves were measured over a shear range of 10^{-3} - 10^{3} s^{-1} and consistency coefficient *K* and flow behavior index *n* were calculated by fitting the curves to the power law equation (1) (Table 1). The consistency coefficient *K* of solutions followed the viscosity trends. For instance, *K* decreased as adding 0.2 % SDS and subsequently increased as the SDS content surpassed its cmc (about 0.25 %). For DTAB and TX-100, *K* decreased as the surfactant content increased. In the case of DTAB, there was only a small difference between the *K* values of 0.6 % and 1.0 % solutions while the *K* values of solutions with TX-100 were similar. This may have been due to the fact that the cmc of DTAB was about 0.5 % and that of TX-100 was about 0.02 %. After reaching the cmc, the further addition of surfactants had little effect on the consistency of the solution. Rheology tests on the solution with 0.01 % TX-100 was conducted to further verify this observation. As shown in Table 1, *K* of the solution was 0.48 – much larger than that of the solutions with 0.2, 0.6, or 1.0 % TX-100.

The *n* indices of all solutions were smaller than 1, indicating shear thinning behavior. A reduced *n* is an indicator of reinforced polymer entanglement, which is essential for electrospinning.[32, 46-49] As shown in Table 1, the flow behavior indices of solutions with SDS decreased while those of solutions with DTAB and TX-100 increased. An increasing amount of SDS facilitated the entanglement of polymers while that of DTAB or TX-100 hindered the electrospinning process. When the content of each surfactant was below its respective cmc, however, the *n* value was smaller than that of the solution without surfactant (0.79). These trends differ from those reported by Kriegel et al. in a similar study.[32] They found that the addition of SDS reduced *n* due to electrostatic attraction between SDS and chitosan, a cationic polymer.

The phenomenon observed can be explained as follows. When the contents were below cmc, the surfactants were in their molecular form and above the cmc, the molecules aggregated together and formed micelles. For DTAB, the cationic surfactant, the micelles interacted with the anionic groups on the lignin (hydroxyl, carboxyl, and sulfonyl) and formed a complex. Since lignin exhibited a highly-branched structure, the complex was likely to be spherical or oval. This destroyed the entanglement between lignin and PVA. The electrostatic repulsion (between SDS and lignin) prevented aggregation similar to the DTAB-lignin complex. On the other hand, the cooperative bonding among SDS, lignin, and PVA reinforced the polymer entanglement and this was why the flow behavior index continued to decrease as the content exceeded cmc.

Surface Tension of the Solution. The surface tension of polymer-surfactant solution as a function of surfactant content is shown in Fig. 3. The PVA-lignin solution exhibited a surface tension of 35.87 mN m^{-1}. The addition of all surfactants significantly reduced the surface tension. In anionic surfactant-containing mixture, the surface tension first decreased to a minimum of 29.79 mN m^{-1} and then increased as a result of reaching the cmc of SDS (0.25 %). When SDS concentration was 1.2 %, the surface tension of the corresponding solution was 31.56 mN m^{-1}. A similar trend was observed for DTAB, lignin, and PVA solutions. The surface tension first decreased to a minimum of 28.39 mN m^{-1} when DTAB concentration was 0.4 % and then increased upon further addition of the cationic surfactant. The addition of TX-100 also greatly decreased the surface tension but larger amounts of TX-100 had little effect in this regard.

Surfactants, regardless of types, all decreased the surface tension of lignin-PVA solution as postulated. The decrease of the surface tension was due to the directional alignment of surfactant molecule on the gas-liquid interface as well as the interaction between the polymers and surfactant. For ionic surfactants (SDS and DTAB), when the content was below cmc, the surfactant molecules were directional aligned on the gas-liquid interface and thus reduced the surface free energy and surface tension of the solution. When surfactant concentration exceeded cmc, the redundant molecules formed micelles. For SDS, the micelles interacted with PVA through cooperative binding and the surface tension was slightly increased. For DTAB, the hydrophilic head group interacted with lignin by electrostatic attraction while the other

hydrophobic one formed cooperative bonds with PVA. The compact lignin-DTAB complex discussed above increased the surface tension. Similar tendencies have been observed by other researchers as well.[30, 34, 46] For non-ionic surfactants, there were two main reasons for the even curve of surface tension versus concentration. On the one hand, the addition amounts were all above cmc because non-ionic surfactants inherently have smaller cmc than ionic ones. On the other hand, there was no interaction among TX-100 and polymers.

Generally, reduction in surface tension benefits the electrospinning of polymer solutions as smaller surface tension allows the polymer to escape the Taylor cone more easily,[1, 50] and the decreased surface tension lowers the required electric field strength for jet initiation. Furthermore, surface tension has a direct effect on the formation of beads and morphology of fibers.[29]

Conductivity of the Solution. Fig. 4 shows the solution conductivity dependence per various surfactant types and concentrations. PVA-lignin solution alone exhibited a conductivity of 9.68 mS cm^{-1}. The continuous incorporation of ionic surfactants (SDS and DTAB) increased the conductivity of the solution while the addition of the non-ionic surfactant (TX-100) had little effect. This difference was expected, as SDS and DTAB ionized in the aqueous solution and provided extra ions thus increasing the conductivity. The enhanced electroconductibility reinforced the electric field strength and benefitted the electrospinning process while preventing bead formation and ensuring smaller fiber sizes.[30]

Fiber Morphology and Diameter. Solution properties including apparent viscosity, rheological properties, surface tension, and conductivity were characterized as discussed above. As hypothesized, the different surfactants had different effects on fiber morphology.

SEM images of nanofibers from the lignin-PVA solution are shown in Fig. 5. In Fig. 5B (2500 ×), some fibers were stuck together forming bundles, and the beaded fibers were also observable in this image. As shown in Fig. 5A (500 ×) and the left bottom side of Fig. 5B, there were many lumps in the electrospun membranes that might have been caused by excess surface tension of the solution. High surface tension made it difficult for the polymers to escape the Taylor cone, and caused the droplet on the tip of the needle to be enlarged as the solution was fed from the syringe. When the solution accumulated to a certain threshold, the droplet ejected from the tip of the needle and electrosprayed on the collector formed lumps.

SEM images of fibers from solutions with surfactants are shown in Fig. 6. All these samples were free of lumps due to the reduced surface tension. The introduction of a small amount of SDS enlarged the beads on the fiber instead of removing them, however the beads disappeared upon further addition of SDS. This was in accordance with the flow behavior index tendency described in Section 3.2. In other words, enhanced polymer entanglement led to the formation of smooth fibers.

For the DTAB and TX-100 counterparts, the incorporation of surfactants at a concentration of 0.2 % entirely eliminated the beaded fibers. Nevertheless, beaded fibers were spun from

solutions with surfactants at higher concentrations. Complexes formed as a result of electrostatic attraction between DTAB and lignin which greatly reduced the polymer entanglement and generated beaded fibers. As shown in Fig. 7, the incorporation of SDS of DTAB reduced the average fiber diameter and its distribution, which could be attributed to the increased surface tension and conductivity. The average diameter of fibers from the lignin-PVA solution was 289.8 ± 69.8 nm while that of fibers from the solution with 0.6 % SDS or DTAB was only 163.5 ± 18.3 and 137.2 ± 27.2 nm, respectively. For TX-100 counterparts, the average fiber diameter and its distribution decreased first and then increased as the content increased. The fiber diameter distribution of fibers with 1.0 % TX-100 was 58.9 nm, which was much larger than those of fibers with SDS and DTAB. This tendency may be attributable to the excess amount of surfactant micelles.[34]

FT-IR of Fibers. FT-IR analysis was conducted to further confirm whether the surfactant had any notable effect on the electrospun fibers.[41] The FT-IR spectra of fibers from different solutions are shown in Fig. 8. The characteristic absorption bands for fibers from pure lignin-PVA solution were as follows. The –OH related peaks included hydrogen bonded –OH at 3350 – 3400 cm^{-1} as well as free –OH at ~2930 cm^{-1}.[51] The peak at ~1135 cm^{-1} is associated with the crystallization of PVA and the primary hydroxyl group in PVA located at ~ 1045 cm^{-1} as well as the C-C bonds in PVA corresponding to the peak at ~850 cm^{-1}.[52] The peak at 1722 cm^{-1} is likely the characteristic absorption of C=O in the lignin side chain or remaining vinyl acetate produced by PVA. Adsorption bands at 1594 and 1505 cm^{-1} are assigned to the aromatic ring skeleton and C-O deformation in primary aliphatic, phenolic, secondary ether while aliphatic –

OH was attached to the peak at 1043 cm^{-1}.[51, 53] All of these peaks indicated that lignin and PVA were successfully spun into nanofibers.

The spectra of fibers prepared from solutions with SDS and DTAB (Fig. 8A) showed a new peak at ~2855 cm^{-1}, which is assigned to the alkyl chain on the surfactants. In addition, as shown in Figs. 8B and 8C, the intensity of the peak increased as the surfactant concentration increased. SDS and DTAB were successfully integrated into the fibers, to this effect. The characteristic vibration was not observed in the spectra of the TX-100 counterparts, possibly due to 1) the non-ionized characteristics of TX-100 or 2) the absence of TX-100 in the fibers as the molecules mostly aggregated in the solution.

DSC and Electrochemical Characterization. The electrospun fibers were subjected to DSC measurements to determine the effects of surfactants on the thermostabilities and microstructures of fibers (i.e., crystallinity). The temperatures of the samples and reference pans were measured as a function of oven temperature to determine the heat flow. All samples exhibited glass transition temperatures (T_g), which represented the degree of orientation in the fiber microstructures. The alkali lignin and PVA exhibited T_g values of ~ 86 and 92 °C, respectively. After being electrospun into fibers, the T_g converted to 152.36 ± 1.17 °C (Table 2), which indicated successful crosslinking between lignin and PVA.[54, 55]

As listed in Table 2, the addition of surfactants (regardless of types or concentrations) elevated the T_g values of the fibers, which indirectly proved the presence of surfactants inside

fibers. In other words, the crystallinity of fibers was improved by the incorporation of surfactants in the electrospinning process. The fiber formed due to enhanced polymer entanglement, reduced surface tension, and increased conductivity (for SDS and DTAB) during electrospinning; these factors altogether improved the orientation of fiber microstructures. Continuously adding SDS and DTAB increased the T_g of the samples while an increased concentration of TX-100 reduced the T_g. When 0.2% SDS or DTAB was added, T_g was 163.75 ± 1.22 and 163.10 ± 1.30 °C, respectively. When the concentration of ionic surfactants was increased to 1%, T_g increased to 169.65 ± 0.52 and 166.40 ± 0.35 °C, respectively. For counterparts of TX-100, as the concentration increased from 0.2 to 1.0%, the T_g value decreased from 158.41 ± 2.34 to 154.18 ± 1.53 °C. This trend was fitted to the transitions of rheological properties, surface tension, and conductivity discussed above.

Electrochemical characterization was performed by using two-electrode symmetrical system in 6M KOH aqueous solution. The CV curves of all samples (Fig. 9A) were quasi-rectangular except for CNF-TX. All CNFs, apart from CNF-TX, showed excellent electrical double-layer capacitive behavior. In Fig. 9A, the CV curve of CNF-SDS has the largest loop area, indicating that it is better suited as a supercapacitor electrode material than the other materials we tested.

The galvanostatic charge-discharge method was adopted to test the performance of the electrochemical capacitors. The charge-discharge curves of different samples were obtained at a constant current density of 1 A g^{-1} with the potential range of 0-1 V in 6M KOH aqueous electrolyte. The charge-discharge curves of CNFs were approximately isosceles, suggesting

favorable capacitive performance. CNF-SDS showed the longest discharging time, i.e., best material capacitance.

The capacitance of each electrode was calculated based on the following equation:

$$C = \frac{2 \times I \times \Delta t}{\Delta V \times m}$$

where I is the discharge current (A), ΔV is the voltage window during the discharge in volt (V), Δt is the discharge time in the selected potential difference in seconds (s), m is the mass of an electrode in grams (g), and C is the gravimetric capacitance (F g^{-1}). The gravimetric capacitance of CNF-C, CNF-SDS, CNF-DTAB, and CNF-TX measured at 1 A g^{-1} was 66.3, 80.7, 62.6, and 34.0 F g^{-1}, respectively. The capacitance improvement in CNF-SDS as compared to CNF-C was attributable to its reduced size and smoother fiber morphology. The decreased diameter and beads of fibers facilitated the ion transportation inside the membrane and provided more pores for ion storage. By contrast, the capacitance of CNF-TX was well below that of CNF-C in accordance with their CV curves. The larger diameter of CNF-TX lowered the surface area so that the storage space for electrolyte ions was reduced as well as capacitance. Furthermore, the existence of beads in CNF-TX impeded the diffusion of electrolyte.[56] The above results together indicated that SDS could not only facilitate the electrospinning of lignin but also improve the electrochemical performance of the carbonized membrane.

CONCLUSIONS

In this study, several kinds of surfactants were incorporated in the electrospinning of lignin by simply adding them into the lignin-PVA solution. It was found that the addition of surfactants

had marked effects on the morphology, magnitude, and nanostructure of the spun nanofibers. Surfactant addition (regardless of type or concentration) eliminated lumps, reduced the average diameter of nanofibers, and enhanced the orientation of fiber microstructures, and adding certain amounts of surfactants formed bead-free fibers with small-diameter distribution. These phenomena were examined by assessing the solution properties. The elimination of beads and reduction of fiber size were attributed to reduction in surface tension and enhanced polymer entanglement. By testing various concentrations, it was observed that the critical micelle concentration (cmc) of surfactants plays an important role in modulating the polymer solution and nanofibers. FT-IR verified the existence of SDS and DTAB in the spun fibers but the incorporation of TX-100 was not observed, as its side chain differed from those of the other two chemicals. The addition of SDS and DTAB did not compromise the electrochemical performance of carbonized nanofiber membranes as supercapacitor electrodes. The efficient modulation of nanofiber morphology and simple, effective electrospinning process without loss of terminal performance may have remarkable commercial potential, as lignin-based and carbon nanofibers are useful in ion batteries, supercapacitors, sensors, and other applications.

ACKNOWLEDGMENTS

This contribution was identified by Prof. Maria Auad (Auburn University, USA) as the Best Presentation in the “Cellulose & Renewable Materials” session of the 2017 ACS Spring National Meeting in San Francisco, CA. We are grateful for the financial support of this research from the Fundamental Research Funds for the Central Universities (2015ZCQ-CL-02),

the National Natural Science Foundation of China (31430092, 31670587), and Program of International S & T Cooperation of China (2015DFG31860).

REFERENCES

(1) Li, D.; Xia, Y. Electrospinning of nanofibers: reinventing the wheel? *Adv. Mater.* **2004**, *16*, 1151-1170.

(2) Greiner, A.; Wendorff, J. H. Electrospinning: A Fascinating Method for the Preparation of Ultrathin Fibers. *Angew. Chem. Int. Edit.* **2007**, *46*, 5670-5703.

(3) Liu, H. A.; Zepeda, D.; Ferraris, J. P.; Balkus, K. J. Electrospinning of poly(alkoxyphenylenevinylene) and methanofullerene nanofiber blends. *ACS Appl. Mater. Inter.* **2009**, *1*, 1958-65.

(4) Lu, P.; Hsieh, Y. L. Multiwalled carbon nanotube (MWCNT) reinforced cellulose fibers by electrospinning. *ACS Appl. Mater. Inter.* **2010**, *2*, 2413-20.

(5) Reneker, D. H.; Yarin, A. L.; Fong, H.; Koombhongse, S. Bending instability of electrically charged liquid jets of polymer solutions in electrospinning. *J. Appl. Phys.* **2000**, *87*, 4531-4547.

(6) Doshi, J.; Srinivasan, G.; Reneker, D. A novel electrospinning process. *Polym. News* **1995**, *20*, 206-13.

(7) Doshi, J.; Reneker, D. H. Electrospinning process and applications of electrospun fibers. *J. Electrostat.* **1995**, *35*, 151-160.

(8) Chuangchote, S.; Jitputti, J.; Sagawa, T.; Yoshikawa, S. Photocatalytic activity for hydrogen evolution of electrospun TiO2 nanofibers. *ACS Appl. Mater. Inter.* **2009**, *1*, 1140-1143.

(9) Wei, Q.; Xiong, F.; Tan, S.; Huang, L.; Lan, E. H.; Dunn, B.; Mai, L. Porous One-Dimensional Nanomaterials: Design, Fabrication and Applications in Electrochemical Energy Storage. *Adv. Mater.* **2017**, *29*, 1602300.

(10) Zhang, P.; Shao, C.; Zhang, Z.; Zhang, M.; Mu, J.; Guo, Z.; Liu, Y. In situ assembly of well-dispersed Ag nanoparticles (AgNPs) on electrospun carbon nanofibers (CNFs) for catalytic reduction of 4-nitrophenol. *Nanoscale* **2011**, *3*, 3357-3363.

(11) Sill, T. J.; von Recum, H. A. Electrospinning: applications in drug delivery and tissue engineering. *Biomaterials* **2008**, *29*, 1989-2006.

(12) Upton, B. M.; Kasko, A. M. Strategies for the Conversion of Lignin to High-Value Polymeric Materials: Review and Perspective. *Chem. Rev.* **2015**, *116*, 2275-2306.

(13) Fang, W.; Yang, S.; Wang, X.-L.; Yuan, T.-Q.; Sun, R.-C. Manufacture and application of lignin-based carbon fibers (LCFs) and lignin-based carbon nanofibers (LCNFs). *Green Chem.* **2017,** *19*, 1794-1827.

(14) Lallave, M.; Bedia, J.; Ruiz-Rosas, R.; Rodriguez-Mirasol, J.; Cordero, T.; Otero, J. C.; Marquez, M.; Barrero, A.; Loscertales, I. G., Filled and hollow carbon nanofibers by coaxial electrospinning of Alcell lignin without binder polymers. *Adv. Mater.* **2007**, *19*, 4292-4296.

(15) Gao, G.; Dallmeyer, J. I.; Kadla, J. F. Synthesis of lignin nanofibers with ionic-responsive shells: water-expandable lignin-based nanofibrous mats. *Biomacromolecules* **2012**, *13*, 3602-10.

(16) Hu, S. X.; Zhang, S. L.; Pan, N.; Hsieh, Y. L. High energy density supercapacitors from lignin derived submicron activated carbon fibers in aqueous electrolytes. *J. Power Sources* **2014,** *270*, 106-112.

(17) Wang, S. X.; Yang, L. P.; Stubbs, L. P.; Li, X.; He, C. B. Lignin-Derived Fused Electrospun Carbon Fibrous Mats as High Performance Anode Materials for Lithium Ion Batteries. *ACS Appl. Mater. Inter.* **2013**, *5*, 12275-12282.

(18) Ruiz-Rosas, R.; Bedia, J.; Lallave, M.; Loscertales, I. G.; Barrero, A.; Rodriguez-Mirasol, J.; Cordero, T. The production of submicron diameter carbon fibers by the electrospinning of lignin. *Carbon* **2010**, *48*, 696-705.
(19) Berenguer, R.; García-Mateos, F.; Ruiz-Rosas, R.; Cazorla-Amorós, D.; Morallón, E.; Rodríguez-Mirasol, J.; Cordero, T. Biomass-derived binderless fibrous carbon electrodes for ultrafast energy storage. *Green Chem.* **2016**, *18*, 1506-1515.
(20) Ago, M.; Jakes, J. E.; Johansson, L. S.; Park, S.; Rojas, O. J. Interfacial properties of lignin-based electrospun nanofibers and films reinforced with cellulose nanocrystals. *ACS Appl. Mater. Inter.* **2012**, *4*, 6849-56.
(21) Lai, C. L.; Zhou, Z. P.; Zhang, L. F.; Wang, X. X.; Zhou, Q. X.; Zhao, Y.; Wang, Y. C.; Wu, X. F.; Zhu, Z. T.; Fong, H. Free-standing and mechanically flexible mats consisting of electrospun carbon nanofibers made from a natural product of alkali lignin as binder-free electrodes for high-performance supercapacitors. *J. Power Sources* **2014**, *247*, 134-141.
(22) Lai, C.; Kolla, P.; Zhao, Y.; Fong, H.; Smirnova, A. L. Lignin-derived electrospun carbon nanofiber mats with supercritically deposited Ag nanoparticles for oxygen reduction reaction in alkaline fuel cells. *Electrochim. Acta* **2014**, *130*, 431-438.
(23) Ago, M.; Jakes, J. E.; Rojas, O. J. Thermomechanical properties of lignin-based electrospun nanofibers and films reinforced with cellulose nanocrystals: A dynamic mechanical and nanoindentation study. *ACS Appl. Mater. Inter.* **2013**, *5*, 11768-11776.
(24) Dallmeyer, I.; Ko, F.; Kadla, J. F. Electrospinning of Technical Lignins for the Production of Fibrous Networks. *J. Wood Chem. Techno.* **2010**, *30*, 315-329.
(25) Dallmeyer, I.; Ko, F.; Kadla, J. F. Correlation of Elongational Fluid Properties to Fiber Diameter in Electrospinning of Softwood Kraft Lignin Solutions. *Ind. Eng. Chem. Res.* **2014,** *53*, 2697-2705.
(26) Seo, D. K.; Jeun, J. P.; Kim, H. B.; Kang, P. H. Preparation and characterization of the carbon nanofiber mat produced from electrospun PAN/lignin precursors by electron beam irradiation. *Rev. Adv. Mater. Sci.* **2011**, *28*, 31-34.
(27) Choi, D. I.; Lee, J.-N.; Song, J.; Kang, P.-H.; Park, J.-K.; Lee, Y. M. Fabrication of polyacrylonitrile/lignin-based carbon nanofibers for high-power lithium ion battery anodes. *J. Solid State Electrochem.* **2013**, *17*, 2471-2475.
(28) Ago, M.; Okajima, K.; Jakes, J. E.; Park, S.; Rojas, O. J. Lignin-based electrospun nanofibers reinforced with cellulose nanocrystals. *Biomacromolecules* **2012**, *13*, 918-926.
(29) Fong, H.; Chun, I.; Reneker, D. Beaded nanofibers formed during electrospinning. *Polymer* **1999**, *40*, 4585-4592.
(30) Lin, T.; Wang, H.; Wang, H.; Wang, X. The charge effect of cationic surfactants on the elimination of fibre beads in the electrospinning of polystyrene. *Nanotechnology* **2004**, *15*, 1375-1381.
(31) Rosen, M. J.; Kunjappu, J. T. *Surfactants and interfacial phenomena*. John Wiley & Sons: 2012; Chapter 1, pp 1-3.
(32) Kriegel, C.; Kit, K. M.; McClements, D. J.; Weiss, J. Electrospinning of chitosan–poly(ethylene oxide) blend nanofibers in the presence of micellar surfactant solutions. *Polymer* **2009**, *50*, 189-200.
(33) Bhattarai, N.; Edmondson, D.; Veiseh, O.; Matsen, F. A.; Zhang, M. Electrospun chitosan-based nanofibers and their cellular compatibility. *Biomaterials* **2005**, *26*, 6176-84.

(34) Jia, L.; Qin, X.-h. The effect of different surfactants on the electrospinning poly(vinyl alcohol) (PVA) nanofibers. *J. Therm. Anal. Calorim.* **2012**, *112*, 595-605.
(35) Jung, Y. H.; Kim, H. Y.; Lee, D. R.; Park, S. Y.; Khil, M. S. Characterization of PVOH nonwoven mats prepared from surfactant-polymer system via electrospinning. *Macromol. Res.* **2005**, *13*, 385-390.
(36) Araújo, E.; Araújo, E.; Nascimento, M.; de Oliveira, H. Electrospinning of Polymeric Fibres: an Unconventional View on the Influence of Surface Tension on Fibre Diameter. *Fibers Text. East. Eur.* **2016**, *24*, 22-29.
(37) Tarasova, E.; Tamberg, K. G.; Viirsalu, M.; Savest, N.; Gudkova, V.; Krasnou, I.; Märtson, T.; Krumme, A. Formation of uniform PVDF fibers under ultrasound exposure in presence of anionic surfactant. *J. Electrostat.* **2015**, *76*, 39-47.
(38) Suslu, A.; Albayrak, A. Z.; Urkmez, A. S.; Bayir, E.; Cocen, U. Effect of surfactant types on the biocompatibility of electrospun HAp/PHBV composite nanofibers. *J. Mater. Sci. - Mater. Med.* **2014**, *25*, 2677-89.
(39) Araújo, E. S.; Nascimento, M. L. F.; de Oliveira, H. P. Influence of triton X-100 on PVA fibres production by the electrospinning technique. *Fibers Text. East. Eur.* **2013**, *21*, 39-43.
(40) Lai, C. L.; Zhou, Z. P.; Zhang, L. F.; Wang, X. X.; Zhou, Q. X.; Zhao, Y.; Wang, Y. C.; Wu, X. F.; Zhu, Z. T.; Fong, H. Free-standing and mechanically flexible mats consisting of electrospun carbon nanofibers made from a natural product of alkali lignin as binder-free electrodes for high-performance supercapacitors. *J. Power Sources* **2014**, *247*, 134-141.
(41) Wongsasulak, S.; Kit, K.; McClements, D.; Yoovidhya, T.; Weiss, J. The effect of solution properties on the morphology of ultrafine electrospun egg albumen–PEO composite fibers. *Polymer* **2007**, *48*, 448-457.
(42) Poursorkhabi, V.; Mohanty, A. K.; Misra, M. Electrospinning of Aqueous Lignin/Poly(ethylene oxide) Complexes. *J. Appl. Polym. Sci.* **2015**, *132*, 41260.
(43) Cabane, B.; Duplessix, R. Organization of surfactant micelles adsorbed on a polymer molecule in water: a neutron scattering study. *J. Phys.* **1982**, *43*, 1529-1542.
(44) Cabane, B. Structure of some polymer-detergent aggregates in water. *J. Phys. Chem.* **1977**, *81*, 1639-1645.
(45) Shirahama, K.; TSUJII, K.; TAKAGI, T. Free-boundary electrophoresis of sodium dodecyl sulfate-protein polypeptide complexes with special reference to SDS-polyacrylamide gel electrophoresis. *J. Biochem.* **1974**, *75*, 309-319.
(46) Kriegel, C.; Kit, K. M.; McClements, D. J.; Weiss, J. Influence of Surfactant Type and Concentration on Electrospinning of Chitosan–Poly(Ethylene Oxide) Blend Nanofibers. *Food Biophys.* **2009**, *4*, 213-228.
(47) Dilamian, M.; Montazer, M.; Masoumi, J. Antimicrobial electrospun membranes of chitosan/poly(ethylene oxide) incorporating poly(hexamethylene biguanide) hydrochloride. *Carbohydr. Polym.* **2013**, *94*, 364-71.
(48) Wongsasulak, S.; Patapeejumruswong, M.; Weiss, J.; Supaphol, P.; Yoovidhya, T. Electrospinning of food-grade nanofibers from cellulose acetate and egg albumen blends. *J. Food Eng.* **2010**, *98*, 370-376.
(49) Wongsasulak, S.; Kit, K. M.; McClements, D. J.; Yoovidhya, T.; Weiss, J. The effect of solution properties on the morphology of ultrafine electrospun egg albumen–PEO composite fibers. *Polymer* **2007**, *48*, 448-457.

(50) Yao, L.; Haas, T. W.; Guiseppi-Elie, A.; Bowlin, G. L.; Simpson, D. G.; Wnek, G. E. Electrospinning and stabilization of fully hydrolyzed poly (vinyl alcohol) fibers. *Chem. Mater.* **2003**, *15*, 1860-1864.
(51) Hu, S. X.; Hsieh, Y. L. Ultrafine microporous and mesoporous activated carbon fibers from alkali lignin. *J. Mater. Chem. A* **2013**, *1*, 11279-11288.
(52) Kubo, S.; Kadla, J. F. The formation of strong intermolecular interactions in immiscible blends of poly (vinyl alcohol)(PVA) and lignin. *Biomacromolecules* **2003**, *4*, 561-567.
(53) Shen, Q.; Zhang, T.; Zhang, W. X.; Chen, S. A.; Mezgebe, M. Lignin-Based Activated Carbon Fibers and Controllable Pore Size and Properties. *J. Appl. Polym. Sci.* **2011**, *121*, 989-994.
(54) Svinterikos, E.; Zuburtikudis, I. Carbon nanofibers from renewable bioresources (lignin) and a recycled commodity polymer [poly (ethylene terephthalate)]. *J. Appl. Polym. Sci.* **2016**, *133*, 43936.
(55) Schreiber, M.; Vivekanandhan, S.; Mohanty, A. K.; Misra, M. Iodine Treatment of Lignin-Cellulose Acetate Electrospun Fibers: Enhancement of Green Fiber Carbonization. *ACS Sustain. Chem. Eng.* **2015**, *3*, 33-41.
(56) Zhang L. L.; Zhao X. S. Carbon-based materials as supercapacitor electrodes. *Chem. Soc. Rev.* **2009,** *38*, 2520-2531.

FIGURE CAPTIONS

Figure 1. Apparent viscosity values of solutions with surfactants of varying types and contents.

Figure 2. Schematic illustration of the incorporation of surfactants into the lignin-PVA solution.

Figure 3. Surface tension values of solutions with surfactants of varying types and contents.

Figure 4. Conductivity values of solutions with surfactants of varying types and contents.

Figure 5. SEM images of nanofibers from the solution without surfactants (A: feeding rate of 1 mL h^{-1}, magnification times 500 ×; B: feeding rate of 1 mL h^{-1}, 2500 ×).

Figure 6. SEM images of fibers from solutions with (A1) 0.2 % SDS, (A2) 0.4 % SDS, (A3) 0.6 % SDS, (A4) 0.8 % SDS, (A5) 1.0 % SDS, (A6) 1.2 % SDS, (B1) 0.2 % DTAB, (B2) 0.4 % DTAB, (B3) 0.6 % DTAB, (B4) 0.8 % DTAB, (B5) 1.0 % DTAB, (B6) 1.2 % DTAB, (C1) 0.2 % TX-100, (C2) 0.4 % TX-100, (C3) 0.6 % TX-100, (C4) 0.8 % TX-100, (C5) 1.0 % TX-100, (C6) 1.2 % TX-100.

Figure 7. Average diameters of nanofibers from solutions with surfactants of varying concentrations (0.2%, 0.6%, 1.0%).

Figure 8. Infrared absorbance spectra of electrospun lignin–PVA–surfactant fibers at wave numbers ranging from 4000 to 600 cm^{-1}. (A) Spectra of fibers without surfactant, with 1.0% SDS, 1.0% DTAB and 1.0% TX-100; (B) spectra of fibers without surfactant, with 0.2% SDS, 0.6% SDS, 1.0% SDS; (C) spectra of fibers without surfactant, with 0.2% DTAB, 0.6% DTAB, 1.0% DTAB; (D) spectra of fibers without surfactant, with 0.2% TX-100, 0.6% TX-100, 1.0% TX-100.

Figure 9. Electrochemical characterizations of carbon fiber membranes from solutions with varying surfactants. (A) CV curves at 50 mv s^{-1}; (B) Galvanostatic charge-discharge curves at 1 A g^{-1}.

TABLES

Table 1. Consistency coefficient *K*, flow behavior index *n* of solutions with surfactants of varying types and contents

Surfactant Concentration (%)	*K*			*n*		
	SDS	DTAB	TX-100	SDS	DTAB	TX-100
0	0.55	0.55	0.55	0.55	0.55	0.55
0.01	-	-	0.48	-	-	0.76
0.2	0.39	0.23	0.11	0.84	0.74	0.90
0.6	0.57	0.07	0.08	0.72	0.84	0.91
1.0	0.62	0.04	0.05	0.70	0.95	0.96

Table 2. Glass transition temperatures (T_g) of samples measured by DSC at a scanning rate of 5 °C min^{-1} from room temperature to 300 °C

Surfactant concentration (%)	T_g (°C)		
	SDS	DTAB	TX-100
0	153.36 ± 1.17	153.36 ± 1.17	153.36 ± 1.17
0.2	163.75 ± 1.22	163.10 ± 1.30	158.41 ± 2.34
0.6	165.01 ± 1.22	163.78 ± 0.47	156.44 ± 0.29
1.0	169.65 ± 0.52	166.40 ± 0.35	154.18 ± 1.53

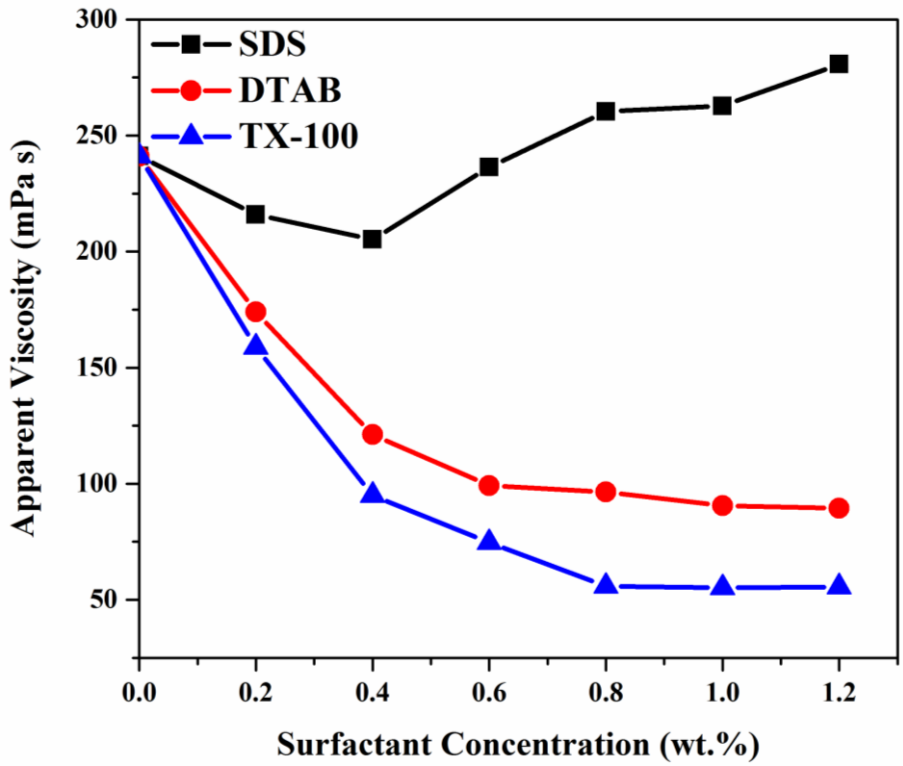
SDS
DTAB
TX-100
Apparent Viscosity (mPa s)
Surfactant Concentration (wt.%)
300
250
200
150
100
50
0.0
0.2
0.4
0.6
0.8
1.0
1.2

Figure 1.

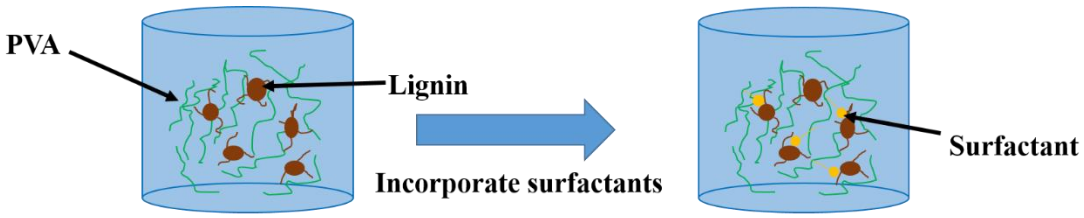

Figure 2.

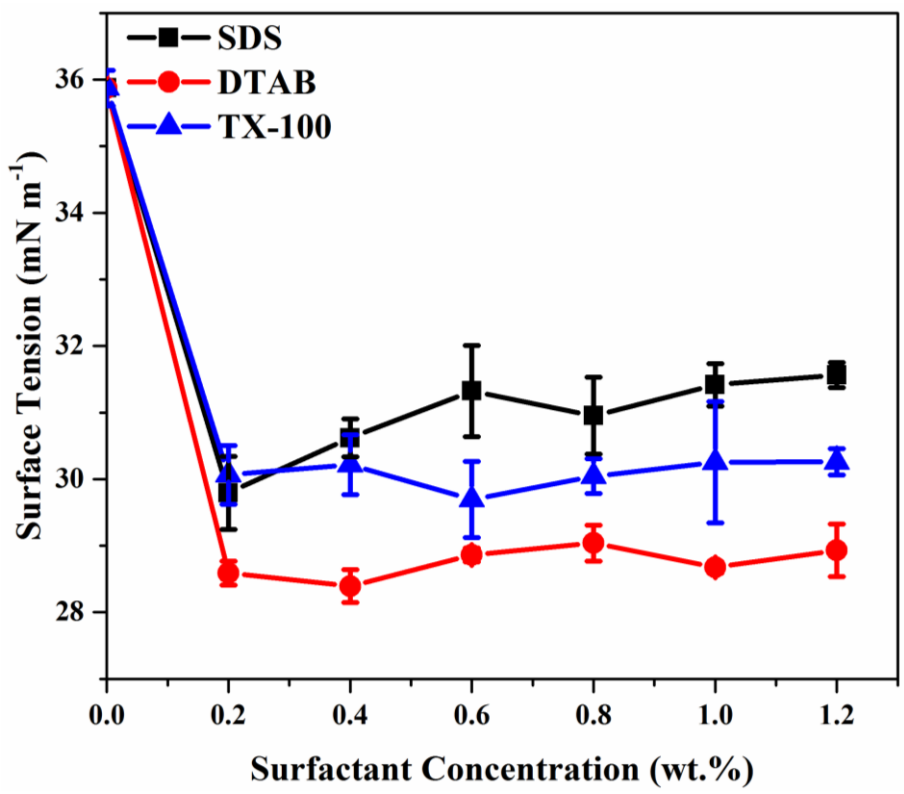
SDS
DTAB
TX-100
Surface Tension (mN m-1)
36
34
32
30
28
0.0
0.2
0.4
0.6
0.8
1.0
1.2
Surfactant Concentration (wt.%)

Figure 3.

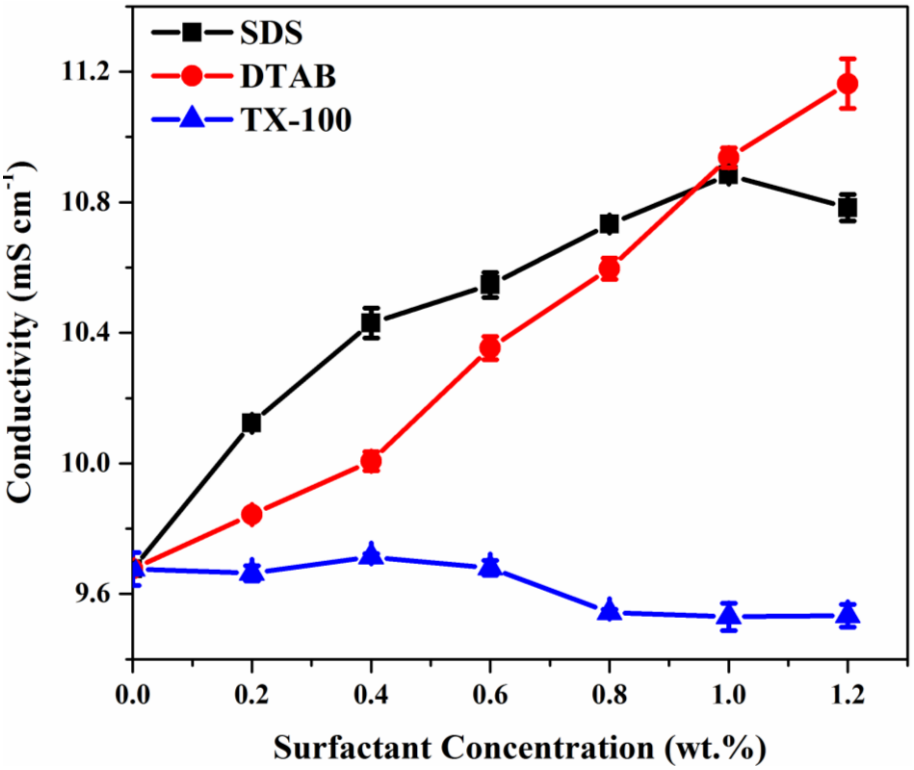
SDS
DTAB
TX-100
Conductivity (mS cm-1)
11.2
10.8
10.4
10.0
9.6
0.0
0.2
0.4
0.6
0.8
1.0
1.2
Surfactant Concentration (wt.%)

Figure 4.

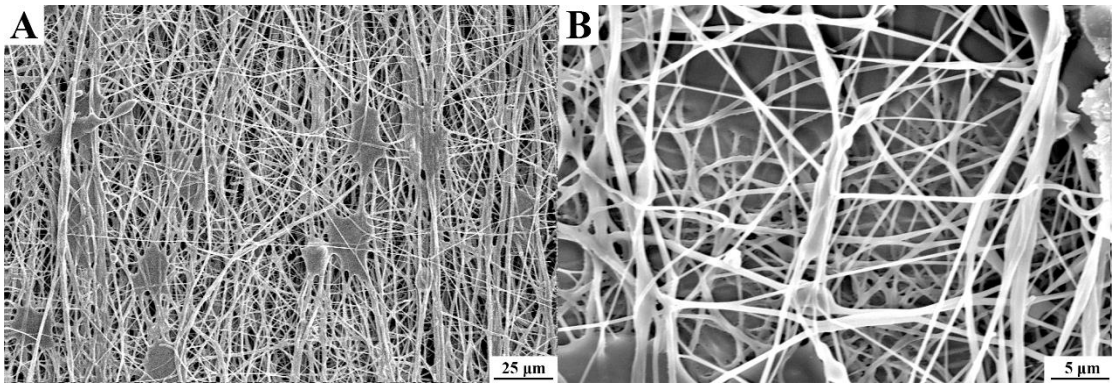

Figure 5.

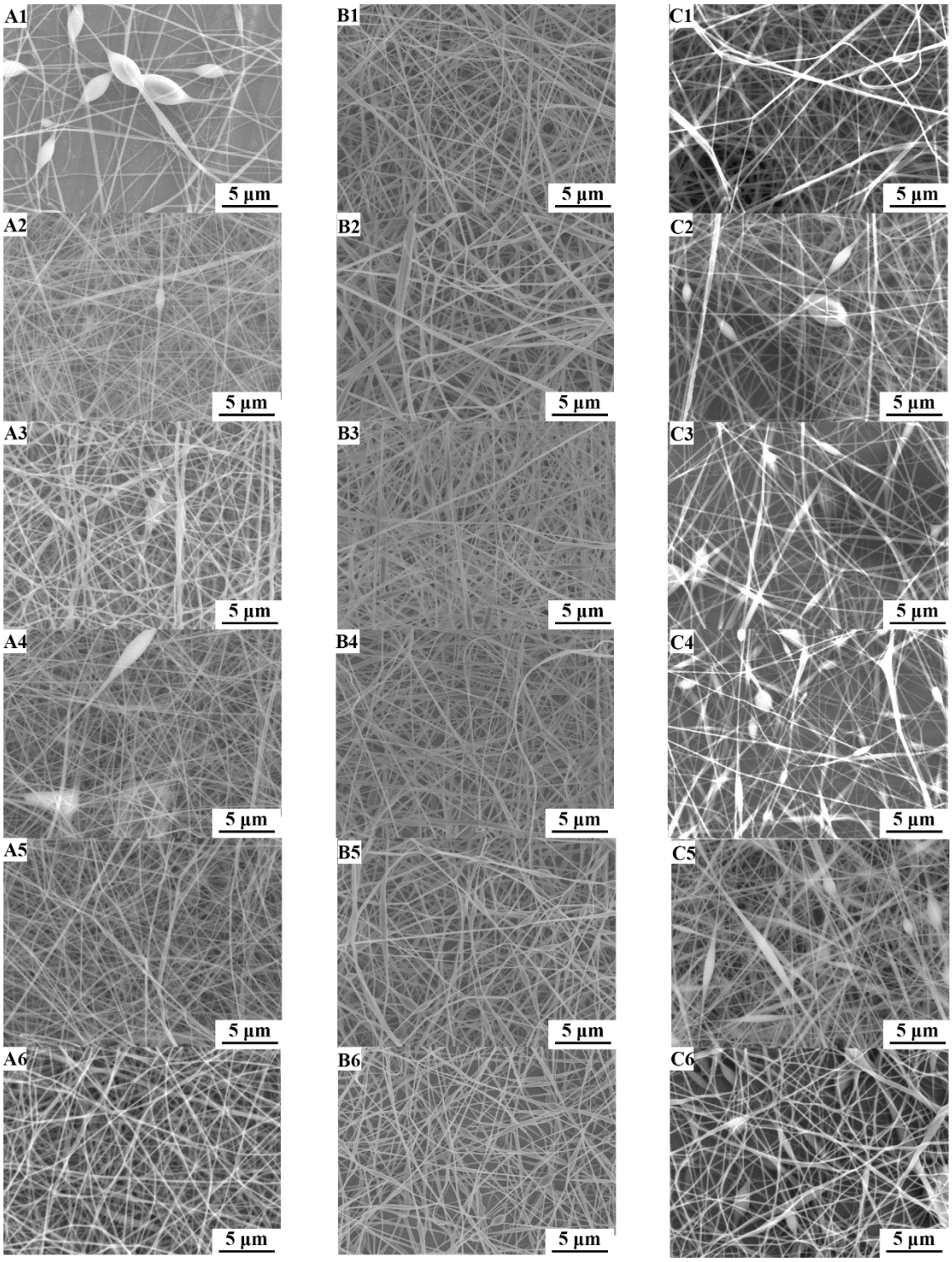
A1
5 µm
B1
5 µm
C1
5 µm
A2
5 µm
B2
5 µm
C2
5 µm
A3
5 µm
B3
5 µm
C3
5 µm
A4
5 µm
B4
5 µm
C4
5 µm
A5
5 µm
B5
5 µm
C5
5 µm
A6
5 µm
B6
5 µm
C6
5 µm

Figure 6.

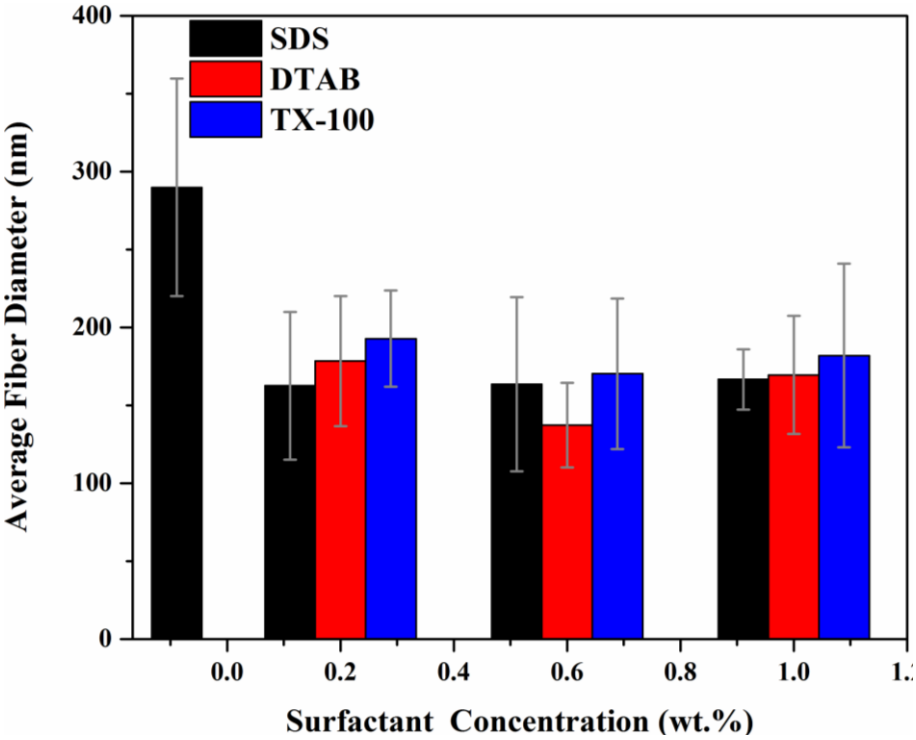
SDS
DTAB
TX-100
Average Fiber Diameter (nm)
400
300
200
100
0
0.0
0.2
0.4
0.6
0.8
1.0
Surfactant Concentration (wt.%)

Figure 7.

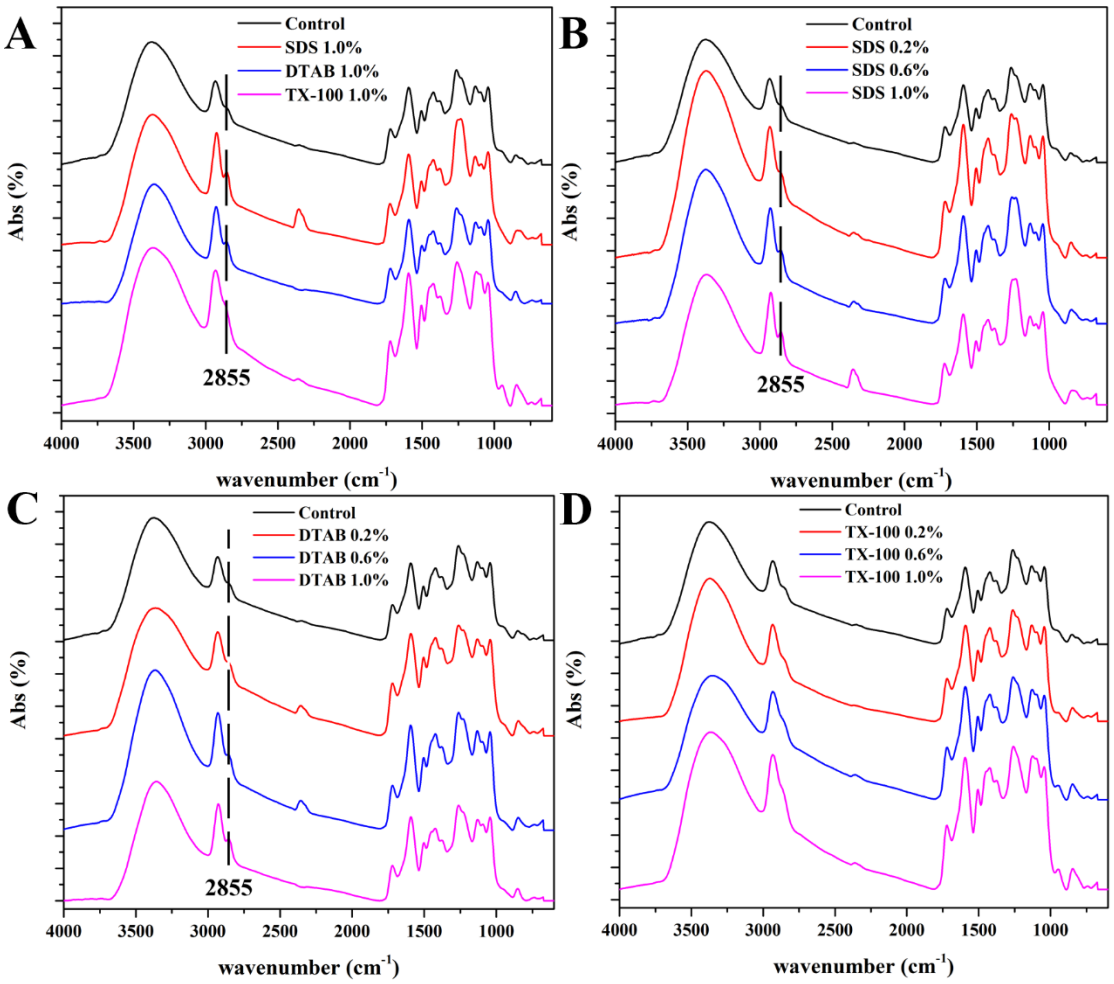
A
Control
SDS 1.0%
DTAB 1.0%
TX-100 1.0%
Abs (%)
2855
4000 3500 3000 2500 2000 1500 1000
wavenumber (cm-1)
B
Control
SDS 0.2%
SDS 0.6%
SDS 1.0%
Abs (%)
2855
4000 3500 3000 2500 2000 1500 1000
wavenumber (cm-1)
C
Control
DTAB 0.2%
DTAB 0.6%
DTAB 1.0%
Abs (%)
2855
4000 3500 3000 2500 2000 1500 1000
wavenumber (cm-1)
D
Control
TX-100 0.2%
TX-100 0.6%
TX-100 1.0%
Abs (%)
4000 3500 3000 2500 2000 1500 1000
wavenumber (cm-1)

Figure 8.

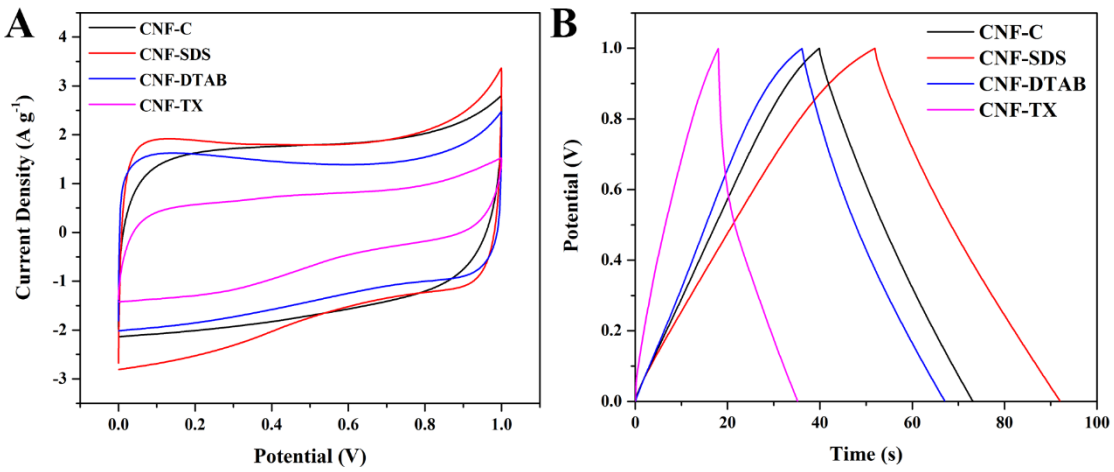
A
CNF-C
CNF-SDS
CNF-DTAB
CNF-TX
Current Density (A g-1)
Potential (V)
B
CNF-C
CNF-SDS
CNF-DTAB
CNF-TX
Potential (V)
Time (s)

Figure 9.

For Table of Contents Only